S_{27}-32
$/6054/$

N93-27753

ρ-ρ ANALYSIS OF A NOVEL NON-CONTACTING
WAVEGUIDE BACKSHORT

T. M. Weller and L. P. B. Katehi,
University of Michigan NASA Center for Space Terahertz Technology
W. R. McGrath,
Jet Propulsion Laboratory Center for Space Microelectronics Technology

ABSTRACT A new non-contacting waveguide backshort has been developed for millimeter and submillimeter wave frequencies. The design consists of a metal bar with rectangular or circular holes cut into it, which is covered with a dielectric (mylar) layer to form a snug fit with the walls of a waveguide. Hole geometries are adjusted to obtain a periodic variation of the guide impedance on the correct length scale, in order to produce efficient reflection of rf power. It is a mechanically rugged design which can be easily fabricated for frequencies from 1 to 1000 GHz and is thus a sound alternative to the miniaturization of conventional non-contacting shorts. To aid in high-frequency design, a rigorous full-wave analysis has been completed which will allow variations of the size, number and spacing of the holes to be easily analyzed. This paper will review the backshort design and the method developed for theoretical characterization, followed by a comparison of the experimental and numerical results. Low frequency models operating from 4-6 GHz are shown to demonstrate return loss of > -0.2 *dB* over a 33% bandwidth. The theory is in good agreement with measured data.

INTRODUCTION

Waveguides are used in a wide variety of applications covering a frequency range from 1 GHz to over 600 GHz. These applications include radar, communications systems, microwave test equipment, and remote-sensing radiometers for atmospheric and astrophysical studies. Components made from waveguides include transmission lines, directional couplers, phase shifters, antennas, and heterodyne mixers, to name a few. In addition to the many commercial applications of waveguides, NASA needs such components in radiometers operating up to 1200 GHz for future space missions, and the Department of Defense is interested in submillimeter wave communications systems for frequencies near 1000 GHz.

One of the most frequent uses of waveguide is as a variable length transmission line. These lines are used as tuning elements in more complex circuits. Such a line is formed by a movable short circuit, or backshort, in the waveguide. A conventional approach is to use a contacting backshort where a springy metallic material, such as beryllium copper, makes DC contact with the broadwalls of the waveguide. The contacting area is critical, however, and must be maximized to produce an acceptable short circuit. These backshorts are excellent in that they provide a good short circuit over the entire waveguide band. The contacting areas can degrade, however, due to wear from sliding friction. It is also extremely difficult to get a uniform contact at frequencies above 300 GHz, where the waveguide dimensions become 0.5 mm x 0.25 mm for the 300-600 GHz band.

An alternative approach is the *non*-contacting backshort shown in Figure 1. A thin dielectric layer (such as mylar) prevents contact and allows the backshort to slide smoothly. In order to produce an rf short and, hence, a large reflection, this backshort has a series of high- and low-impedance sections which are approximately $\frac{\lambda_g}{4}$ in length, where λ_g is the guide wavelength. The rf impedance of this design is given approximately by [1]

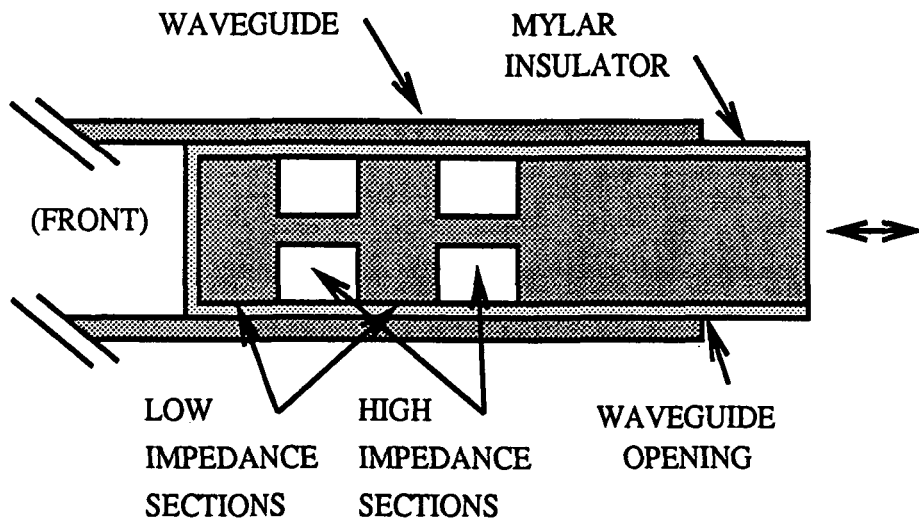$$Z_{rf} = (\frac{Z_{low}}{Z_{high}})^n Z_{low} \qquad (1)$$

Figure 1: Cross sectional view of a conventional non-contacting backshort.

where Z_{low} is the impedance of the thick (low-impedance) sections, Z_{high} is the impedance of the thin (high-impedance) sections, and n is the number of sections. Beginning near 100 GHz, the thin high-impedance sections become difficult to fabricate, and fabrication may not even be feasible beyond 300 GHz. It would also be difficult to have the short slide snugly inside the waveguide at these high frequencies, as the thin sections would be very weak. To circumvent these problems, a novel non-contacting backshort design has recently been developed [2, 3] which is suitable for millimeter and submillimeter wave operation. It is a mechanically rugged design which can be easily fabricated for frequencies from 1 to 1000 GHz, and is thus a sound alternative to the miniaturization of conventional non-contacting shorts. Previously, however, the new backshort was optimized empirically using low-frequency models. This paper will discuss the new design and outline a new method developed for theoretical characterization. The formulation is a rigorous full-wave analysis which involves both mode-matching techniques and a coupled set of space domain integral equations. A description of the experimental setup is included, followed by a comparison of experimental and theoretical results. The new theoretical formulation fits these results well.
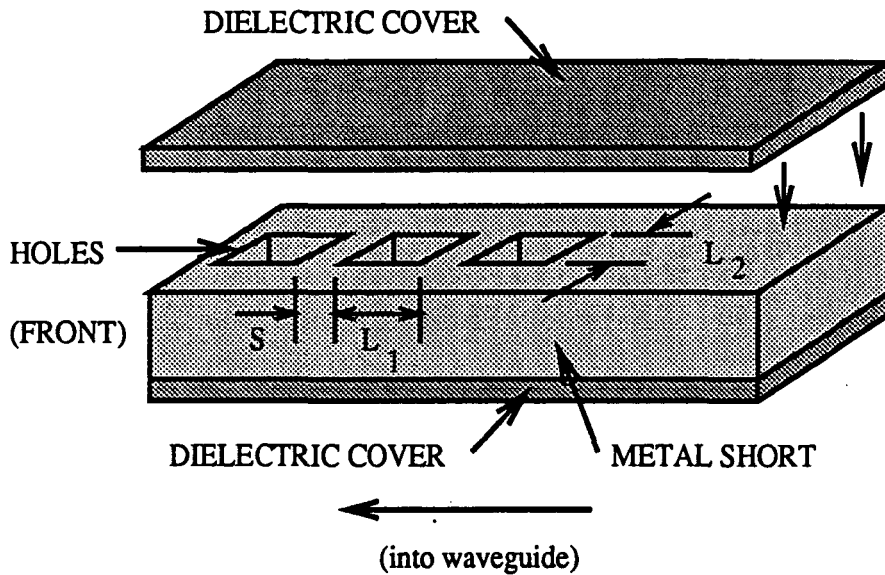
Figure 2: The new non-contacting backshort design, shown with three rectangular holes. The size, shape, and spacing of these holes are important in determining the rf properties of the short. S is the spacing, L_1 is the length, and L_2 is the width of each hole. The front of the backshort is inserted into the waveguide opening.

NOVEL NON-CONTACTING BACKSHORT DESIGN

The novel non-contacting backshort has the merits of easy fabrication up to Thz frequencies, flexibility of design, and very good performance over relatively broad bandwidths. The important features are briefly reviewed here. In order to obtain a large reflection, a non-contacting backshort must provide a periodic variation of guide impedance on the correct length scale. This is accomplished in the new design by either rectangular or circular holes, with the proper dimensions and spacing, cut into a metallic bar. A representative design is shown in Figure 2. This bar is sized to fill the waveguide cross-section and slide smoothly with a dielectric (mylar) insulator along the broadwalls. The holes replace the thin-metal, high-impedance sections in the conventional design shown in Figure 1. Since the holes extend completely through the bar, this yields a higher impedance than the corresponding sections in the conventional design. Thus, the high-to-low impedance ratio is larger in the new design. In addition, the electromagnetic fields are concentrated near the central axis of

calculated return loss for a backshort with no holes, inserted about 4.5 inches into the end of the waveguide, and covered with mylar ($\epsilon_r = 3.35$). The waveguide opening is assumed to present a 0 Ω impedance (i.e., it is covered with a metallic plate). Although the gap height is only 2.5% of the waveguide height, roughly 65% of the incident power is lost at resonance due to finite conductor and dielectric loss. The utility of the holes, then, is to minimize or eliminate these dropouts.

THEORETICAL CHARACTERIZATION

The theoretical characterization of the JPL backshort design is performed using a combination of two well known full-wave analysis methods, namely mode-matching and the application of equivalent magnetic currents in a space domain integral equation. In what follows, the approach will be outlined and the major governing equations presented. It is noted here that the symmetry of the backshort about the x-z plane (parallel to the plane of the waveguide broadwalls) has been utilized to reduce the number of unknown parameters. Furthermore, only rectangular holes (not round) have been considered in order to simplify the analysis. Neither of these points, however, are necessary restrictions in the formulation.

A discussion of the analysis is aided by the schematic in Figure 4, which represents the cross-sectional view of a backshort with two holes, inserted a distance d into the end of a rectangular waveguide. The structure is symmetric about the x-z plane, with equal dielectric regions (which are the dielectric covers shown in Figure 2) above and below the metal short. The problem of interest is to determine the reflection coefficient for the dominant waveguide mode, travelling in the $+z$ direction, at the front of the backshort ($z = 0$).

The formulation is based on the decomposition of the problem into two primary components. In the first part, we wish to compute the scattering matrix $[S]$ at $z = 0$, as depicted in Figure 4. As $[S]$ represents simply the scattering at a waveguide discontinuity, the presence of the holes may be neglected and thus becomes decoupled from the problem at hand. The
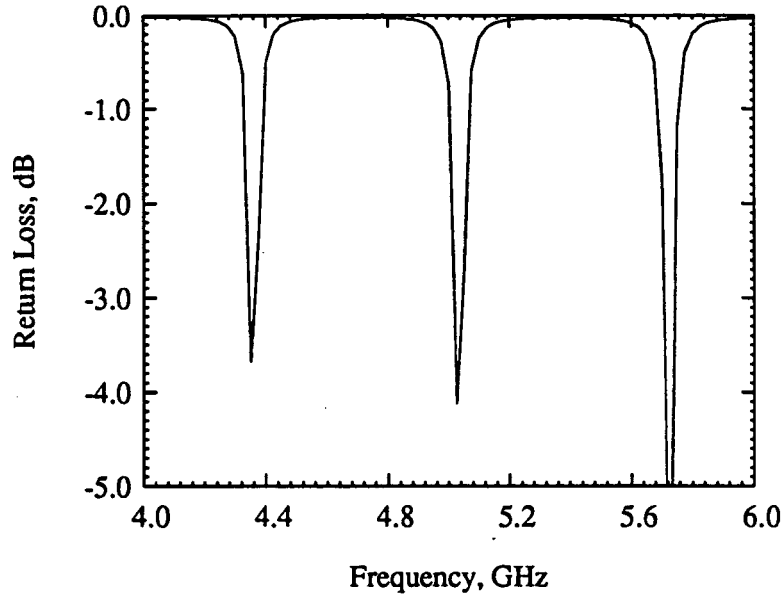
Figure 3: Calculated return loss versus frequency for a backshort with no holes, where the gap height is 2.5% of the total guide height.

the waveguide, such that the holes are effective in producing large correlated reflections, and thus acting as an efficient rf short. The new design is also easy to fabricate and can be used at any frequency between 1 GHz and 1000 GHz. For very high frequencies, above 300 GHz, the metallic bar is a piece of shim stock polished to the correct thickness. The holes can be formed by drilling, punching, or laser machining, or they can be etched using common lithography techniques.

It is important to note that the holes are a *critical* factor in obtaining efficient reflection from the non-contacting short. With the backshort inserted in the waveguide, a cavity forms between the metal bar and the broadwall of the waveguide, in the region occupied by the dielectric insulator. This cavity is terminated by the large discontinuities at the front of the short and at the waveguide opening. (This is more clearly illustrated in Figure 1 for the conventional design.) Deep dropouts in the return loss will occur at frequencies for which this cavity resonates, even though the height of each gap may be only a small fraction of the total waveguide height. The effect is well illustrated in Figure 3, which shows the
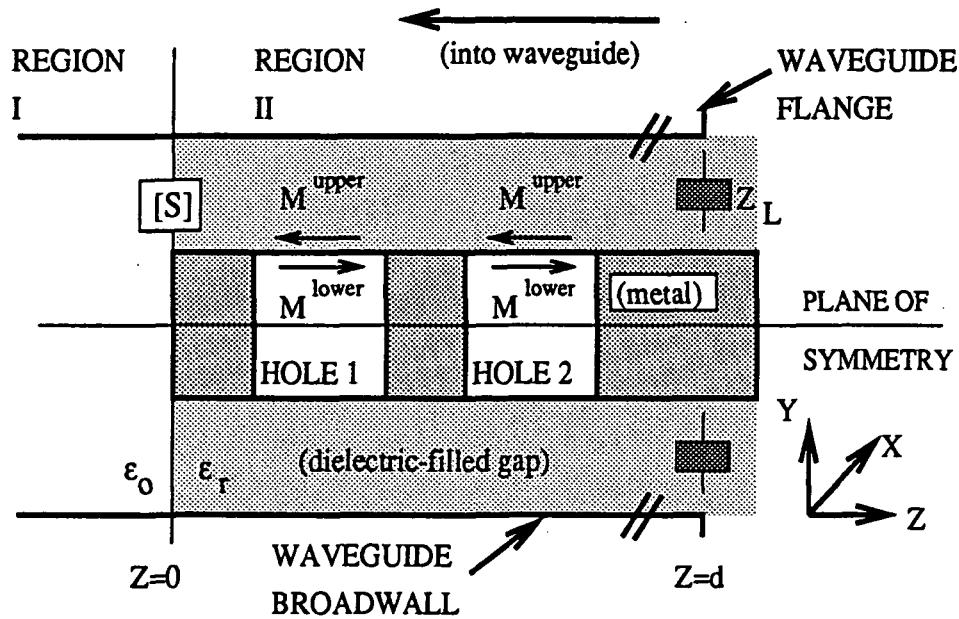
Figure 4: Cross-sectional schematic diagram (not to scale) of a two-hole non-contacting backshort, inserted a distance d into the end of a waveguide. The waveguide broadwalls are on the top and bottom in the figure.

well documented mode-matching method, which has been used to solve a variety of waveguide problems [4, 5, 6] is applied to determine [S]. With this method, the fields at each side of the reference plane ($z = 0$) are expanded in infinite series of orthogonal mode pairs (e.g. TE-to-z and TM-to-z), and continuity of the tangential electric and magnetic fields is enforced to determine the scattered field amplitudes. This results in the following set of generalized equations,

$$\sum_{n,m}^{\infty}(a_e^I + b_e^I)\vec{\Phi}_e^{E,I} + \sum_{n,m}^{\infty}(a_m^I + b_m^I)\vec{\Phi}_m^{E,I} = \sum_{n,m}^{\infty}(a_e^{II} + b_e^{II})\vec{\Phi}_e^{E,II} + \sum_{n,m}^{\infty}(a_m^{II} + b_m^{II})\vec{\Phi}_m^{E,II} \qquad (2)$$

$$\sum_{n,m}^{\infty}(a_e^I - b_e^I)\vec{\Phi}_e^{H,I} + \sum_{n,m}^{\infty}(a_m^I - b_m^I)\vec{\Phi}_m^{H,I} = \sum_{n,m}^{\infty}-(a_e^{II} - b_e^{II})\vec{\Phi}_e^{H,II} + \sum_{n,m}^{\infty}-(a_m^{II} - b_m^{II})\vec{\Phi}_m^{H,II} \qquad (3)$$

where (2) satisfies continuity of tangential $\vec{E}$ and (3) satisfies continuity of tangential $\vec{H}$. In the above, a and b represent the coefficients for waves travelling toward and away from the reference plane, respectively. The subscripts e and m are for TE-to-z and TM-to-z, while

the superscripts denote the field type (electric or magnetic) as well as the region to which they pertain (to the left or right of the reference plane). The vector functions Φ contain the appropriate constants and x- and y-dependencies for the transverse components of the respective fields. At this point inner-products are formed using $\vec{\Phi}_e^{E,I}$ and $\vec{\Phi}_m^{E,I}$ with (2), and $\vec{\Phi}_e^{H,II}$ and $\vec{\Phi}_m^{H,II}$ with (3). As these inner-products involve integration over the guide cross-section, a system is linear equations results due to the orthogonality of the modal components. This system is assembled into a matrix representation and, after inversion, the solution is expressed as

$$\{b\} = \{a\}^T [S] \tag{4}$$

With $[S]$ determined, the unknown scattered-field amplitudes $\{b\}$ are found from (4) given the known incident-field amplitudes, $\{a\}$. It is noted that the presence of a termination at $z = d$ (see Figure 4) is easily accounted for by assigning

$$b^I = a^I S_{11} + a^I S_{12}(I - \Gamma_L S_{22})^{-1}\Gamma_L S_{21}, \tag{5}$$

where I is the identity matrix and $[\Gamma_L]$ is a matrix which accounts for the reflection at $z = d$. As shown in the figure, we assume that the waveguide opening is terminated in a complex load Z_L for simplification. (This approximation is necessary because the conditions outside the short are difficult to control experimentally and, likewise, difficult to accurately characterize analytically. This will be discussed further in the section on results.) The matrix $[\Gamma_L]$ is thus a diagonal matrix of elements

$$(\Gamma_L)_{i,i} = \frac{Z_L - Z_g^i}{Z_L + Z_g^i}e^{-2\gamma_z^i d} \tag{6}$$

In (6), Z_g^i and γ_z^i are the guide impedance and propagation constant, respectively, for the ith TE/TM mode. Conductor and dielectric loss may be included in the factor γ_z^i.

The second principle step in the formulation is to apply the space domain integral equation technique to solve the boundary value problem at the aperture of each of the holes. The

introduction of the equivalent magnetic currents, $\vec{M}^{upper}$ and $\vec{M}^{lower}$ (see Figure 4), allows the hole openings to be closed by an imaginary metallic surface, provided that no natural boundary conditions are violated. This is a crucial step in that it transforms the backshort structure into a combination of a simple rectangular waveguide, which is the dielectric-filled gap region, and a series of isolated metallic cavities, which are the holes. These unknown magnetic currents radiate electromagnetic fields in the dielectric region, and a modified form of (5) therefore results when treating a backshort with holes. The new expression is

$$b^I = a^I S_{11} + a^I S_{12}(I - \Gamma_L S_{22})^{-1}\Gamma_L S_{21} +$$

$$\{(F^> \Gamma_L + F^<)S_{22}(I - \Gamma_L S_{22})^{-1}\Gamma_L + F^> \Gamma_L + F^<\}S_{21}. \tag{7}$$

Note that the only unknown variables in this equation are $F^<$ and $F^>$, as the components of the matrix $[S]$ and $[\Gamma_L]$ have previously been determined. These unknown components are functions of the imposed equivalent magnetic currents.

The solution for the unknown surface currents is uniquely determined by enforcing continuity of the total tangential fields across the hole apertures. This insures that the natural boundary conditions of the original problem are preserved. Continuity of the tangential electric field is satisfied immediately by setting $\vec{M}^{upper} = -\vec{M}^{lower} = \vec{M}$. Assuming a backshort with N holes, continuity of the magnetic field at the kth hole leads to the following space domain integral equation (SDIE) in the unknown $\vec{M}$:

$$-\hat{n} \times \vec{H}^{inc} = \hat{n} \times \{\vec{H}^{scat} +$$

$$\sum_{n=1}^{N}\left(\int\int_{S_n} ds'(\frac{j}{\omega\epsilon\mu}(k^2\bar{\bar{I}} + \nabla\nabla)\cdot\bar{\bar{G}}_B)\cdot\vec{M}_n\right) +$$

$$\int\int_{S_k} ds'(\frac{j}{\omega\epsilon_o\mu}(k^2\bar{\bar{I}} + \nabla\nabla)\cdot\bar{\bar{G}}_C)\cdot\vec{M}_k\} \tag{8}$$

In the above, $\vec{H}^{inc}$ represents the known incident magnetic field, which results from scattering of the incoming wave at the waveguide step discontinuity (the reference plane). It is expressed

in terms of TE and TM modes, the coefficients being given by

$$a^{II} = a^I S_{12}(I - \Gamma_L S_{22})^{-1}\Gamma_L$$

$$b^{II} = a^{II}S_{22} \tag{9}$$

for $+z$ and $-z$ travelling waves, respectively. $\bar{\bar{G}}_B$ and $\bar{\bar{G}}_C$ represent the dyadic Green's functions for an infinite rectangular waveguide and a metallic cavity, respectively. Closed-form expressions for these functions can be derived using well established boundary value formulations [7]. The use of an infinite-waveguide potential in the dielectric-filled gap region, which does not account for the actual finite length of uniform guide, is possible by considering the fields to be a superposition of *primary* and *scattered* components. The primary components satisfy boundary conditions at the source, and radiate away from $\vec{M}$ in the presence of matched conditions in either direction. These components are precisely those of the second term on the right hand side of (8). The scattered components are required to satisfy the boundary conditions away from the source, at the discontinuities at $z = 0, d$ and are also functions of $\vec{M}$. Expressions for these fields, which are represented by $\vec{H}^{scat}$ in (8), are similar in form to the primary components but also include factors from the scattering matrix $[S]$ and the matrix $[\Gamma_L]$.

The final step in the formulation is to solve the coupled set of integral equations which results from enforcing (8) over all N holes. This set may be reduced to a system of linear equations by applying the method of moments (Galerkin's method) [8]. This approach has been proven to yield excellent results and the convergence characteristics have been well documented [9, 10, 11]. Using this procedure, the aperture of each hole is first divided into discrete subsections using a rectangular grid. The unknown currents are then expanded in terms of overlapping subsectional rooftop basis functions of the form,

$$\vec{M} = \sum_{ij} \left(\hat{x}M_{ij}^x f_j(x')\phi_i(z') + \hat{z}M_{ij}^z \phi_j(x')f_i(z')\right) \tag{10}$$

$$f_n(w') = \begin{cases} \frac{sin[k\ (w'-w_{n-1})]}{sin(k\ l_n)} & \text{if } w_{n-1} < w' < w_n \\ \frac{sin[k\ (w_{n+1}-w')]}{sin(k\ l_n)} & \text{if } w_n < w' < w_{n+1} \end{cases}$$

$$\phi_n(w') = \begin{cases} 1 & \text{if } w_{n-1} < w' < w_{n+1} \\ 0 & \text{else} \end{cases}$$

where M_{ij}^x and M_{ij}^z are constant coefficients, l_n is the length of the nth subsection in the w-direction, and k is the wave number in the medium. This expansion is inserted into the integral equation, and inner-products are then formed using weighting functions which are identical to the basis functions. The coupled equations are thereby reduced to the following matrix form:

$$\begin{pmatrix} \langle Y_{xx} \rangle & \langle Y_{xz} \rangle \\ \langle Y_{zx} \rangle & \langle Y_{zz} \rangle \end{pmatrix} \begin{pmatrix} \{M^x\} \\ \{M^z\} \end{pmatrix} = \begin{pmatrix} -\{\tilde{H}_x^{inc}\} \\ -\{\tilde{H}_z^{inc}\} \end{pmatrix} \qquad (11)$$

where $\langle Y_{\zeta\xi}(\zeta,\xi = x,z) \rangle$ represents blocks of an admittance matrix. The unknown current co-efficient vectors $\{M_{ij}^x\}$ and $\{M_{ij}^z\}$ are then determined by solving (11). With $\vec{M}$ determined, all elements of (7) may be computed and the solution is complete.

MEASUREMENT TECHNIQUES

The backshort design was optimized by testing the performance in WR-187 band wave-guide (3.16 GHz - 6.32 GHz), for which the dimensions are 47.5 mm x 22.1 mm. The dielectric layer around the metal short was formed by stacking sheets of mylar tape. The magnitude and phase of the reflection coefficient were measured with an HP 8510B Vector Network Analyzer. A commercially available coaxial-to-waveguide transition connected the waveguide to the network analyzer. This measurement system was calibrated using two off-set contacting shorts set at $\frac{\lambda_g}{8}$ and $\frac{3\lambda_g}{8}$, and a sliding waveguide load. Subsequent verification using a contacting short indicated a measurement error of about $\pm 0.2\ dB$ in the magnitude measurement.

RESULTS AND DISCUSSION

This section presents examples of measured data and analytical calculations. It will also address some conclusions drawn regarding the theoretical characterization and performance of the new design. Regarding the numerical aspects, the code developed to calculate the scattering matrix $[S]$ at the waveguide discontinuity agreed very well with results found in [12]. In particular, results were compared for the reflection coefficient from asymmetric (i.e., single-step) E-plane and H-plane waveguide junctions. The validation of the remainder of the theoretical formulation and the associated software was completed by comparison with measured data. Part of this validation included a study of convergence as a function of the hole (aperture) mesh size and the number of modes used in the dyadic Green's function expansions. It was found that using subsections which are approximately $\frac{\lambda_g}{16}$ on a side, where λ_g is the guide wavelength, yields a good compromise between accuracy and the requirements on storage and computation time. The number of modes for the Green's functions is kept ≥ 600.

The measurements performed to investigate the new design involved many variations on the size, shape, number, and spacing of the holes cut into the metal bar [2]. An additional test variable was the number of stacked mylar sheets used to form the dielectric layer. In many cases, the height of the backshort was such that a relatively large space was left between either side of the metal bar and the waveguide broadwalls. This large gap, combined with the variations in the mylar thickness, are used to help understand the effect that typical machining tolerances will have for operation at 200-300 GHz and above.

Results which are typical of the best performance to date are given in Figure 5b. This data is for a backshort with three rectangular holes, each with dimensions $L_1 = 19.3$ mm, $L_2 = 28.4$ mm and spacing $S = 8.7$ mm. The width and height of the bar are 47.5 mm and 19.7 mm, respectively, leaving a gap of 1.2 mm between the bar and the waveguide broadwalls. The measured results in Figure 5b were obtained using a total mylar thickness
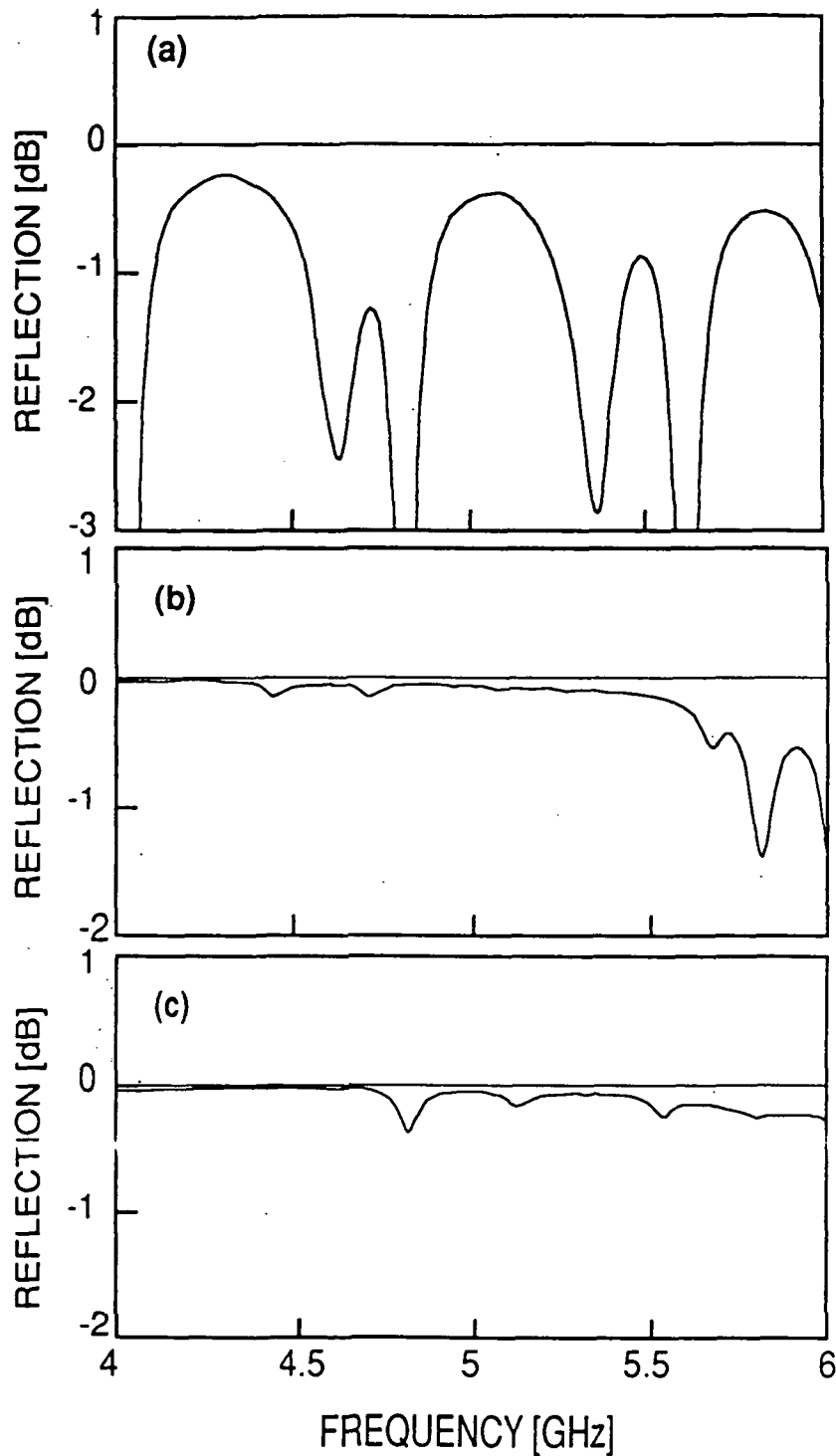
Figure 5: a) Reflected power measured from a solid bar without holes. This does not make a good backshort due to the several large dropouts across the frequency band. b) Reflected power measured from a backshort with three rectangular holes. The mylar is 0.89 mm thick. Excellent performance is obtained over a broad bandwidth. c) Same backshort as in (b), but mylar thickness has been reduced to 0.64 mm.

of 0.89 mm. The reflection coefficient in this case is greater than −0.2 *dB* (0.95 reflected power) over a 33% bandwidth centered around 4.8 GHz. For comparison, the measured results for the same backshort *without* holes are shown in Figure 5a. This data clearly illustrates the improvement from the holes. The complex structure of this response, relative to that shown in Figure 3, is caused by asymmetrical positioning of the bar inside the waveguide. Other measurements made with the gap completely filled by dielectric, which forced a near-symmetric positioning of the bar, agreed very well with our theory and were of the form shown in Figure 3. The effect of reducing the mylar thickness is seen in Figure 5c, which gives measured data using 0.64 mm of mylar. The large dropout near 5.8 GHz has been shifted out of band, due to the decrease in the effective dielectric constant. This response is comparable to that obtained for the conventional type of backshort shown in Figure 1. As expected, increasing the mylar thickness (and thus increasing the effective dielectric constant) moved the large dropouts lower in frequency.

Performance similar to that with rectangular holes could be obtained using circular holes. Results obtained with 3 circular holes and a mylar thickness of 0.89 mm demonstrated greater than 95% reflected power over a 32% bandwidth centered around 4.75 GHz. This is encouraging since round holes are easier to fabricate than rectangular holes for high frequencies.

Many other variations of the backshort parameters were tested. Also, the small dips around 4.5 GHz in Figure 5b, and those seen in Figure 5c, are currently being investigated. As noted for the plain metal bar, these dips may result from asymmetrical positioning of the backshort inside the waveguide [13]. A more extensive discussion of the systematic parameter variations, measurement observations, and comparisons with theory will be given at a later date. Some millimeter wave tests have also been performed and are discussed elsewhere [2].

In order to theoretically model the backshort performance, appropriate values were required for an effective dielectric constant, ϵ_r, and the terminating load impedance for the waveguide opening (Z_L in Figure 4). The problem of the dielectric constant arises because

the gap above and below the metal bar is only partially, and non-uniformly, filled by the mylar sheets. The transverse resonance technique [4] may be used to approximate ϵ_r by solving the exact inhomogeneous problem, and then assuming the entire guide is filled with some "average" material. (For the inhomogeneous case, a two-layer guide is assumed, where one layer is air-filled and the other is mylar-filled and of a thickness equal to the total mylar thickness.) A simpler approach, which yields higher values for the dielectric constant, is to merely compute ϵ_r based on the percentage of mylar relative to the total gap height. By numerical experimentation, it was found that the best approximation lies nearly midway between the two values. It is noted that obtaining an exact solution for a layered waveguide is not justified due to the unpredictable spacing of the various mylar sheets.

The other issue was determining the correct value for the load impedance, Z_L, to use in the calculations. Although an exact analysis is a formidable task, an approximate load impedance can be obtained to adequately model the waveguide discontinuity. This is done by first considering the exact impedance for a very thin aperture opening onto an infinite ground plane. For typical gap dimensions used here, this is a large, capacitive value, with real and imaginary parts which are both 3-5 times the dominant waveguide mode impedance. The extension of the backshort beyond the waveguide opening, however, will provide a better transition to free-space and effectively lower this impedance toward a better match. In many test cases, use of a normalized load impedance of $Z_L \approx 2.5 \pm .5 + j1$ in equation (6) yielded good agreement with the measured results. An important point, however, is that the predicted performance is nearly independent of Z_L in precisely the frequency bands where the backshort works well. This is as expected, as most of the incident power is reflected and never reaches the end of the guide. It follows that changes in Z_L do modify the dropout regions in the return loss, as these dropouts result from out-of-band power leaking past the backshort. (The performance of the bar without holes is likewise strongly dependent on Z_L. This fact can be used in determining an appropriate impedance for a given geometry, by
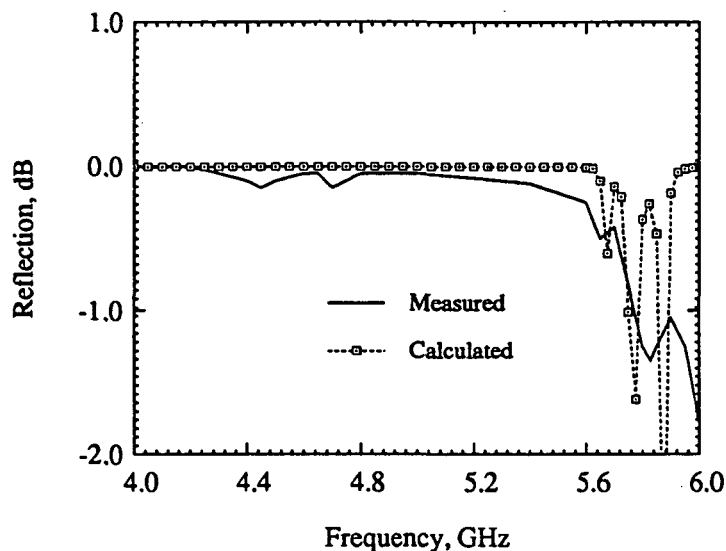
Figure 6: Measured data and calculated performance for the backshort with three rectangular holes. The mylar thickness is 0.89 mm.

comparing measured and theoretical results for various load values.)

A comparison between measured data and calculated performance is given in Figure 6. These results are for the backshort with three rectangular holes, using a mylar thickness of 0.89 mm. Very good agreement has been obtained. The broadening of the dropouts in the measured data, relative to the calculated results, is believed to be due Z_L and to loss in the measurement system which is not accounted for by the theory. The bandwidth is very accurately predicted, however, such that it should now be possible to design and analyze these backshorts for specific applications.

CONCLUSIONS

In summary, we have developed a theoretical analysis to predict the rf performance of a new non-contacting waveguide backshort. This backshort consists of a metallic bar with rectangular or circular holes which enhance the reflections of rf power. The simplicity of this design allows it to be easily scaled to millimeter wave and submillimeter wave frequencies. The new theoretical development is a rigorous full-wave analysis which employs a coupled set of space-domain integral equations and mode-matching techniques. Comparison between

theory and experiment on model backshorts optimized for best performance at 4-6 GHz show very good agreement.

ACKNOWLEDGEMENTS

References

[1] Collin, R. E. *Foundations for Microwave Engineering*, New York: McGraw-Hill, 1966, pp. 259-262.

[2] McGrath, W. R. "A Novel Non-Contacting Waveguide Backshort for Millimeter and Submillimeter Wave Frequencies," *Conference Proceedings of the Second National Technology Transfer Conference*, NASA Conference Publication 3136, Vol. 1, pp. 161-168, December 1991.

[3] McGrath, W. R. "Non-contacting Waveguide Backshort," U.S. Patent pending.

[4] Itoh, Tatsuo (editor). *Numerical Techniques for Microwave and Millimeter-Wave Passive Structures*, John Wiley & Sons, 1989.

[5] Eleftheriades, G. V., Ali-Ahmad, W. Y., Katehi, P. B., and Rebeiz, G. M. "Millimeter-Wave Integrated-Horn Antennas: Part I - Theory", *IEEE Trans. A.P.* , vol. 39 , No. 11, November 1991, pp. 1575-1581.

[6] Masterman, P. H. and Clarricoats, P. J. B. "Computer field-matching solution of waveguide transverse discontinuities", *Proc. IEE*, vol. 118 , No. 1, January 1971, pp. 51-63.

[7] Collin, R. E. *Field Theory of Guided Waves*, Piscataway, NJ: IEEE Press, 1991, pp. 78-86.

[8] Harrington, R. F. *Field Computations by Moment Methods*, New York: Macmillan, 1968.

[9] Dib, N. I., Katehi, P. B., Ponchak, G. E., and Simons, R. N. "Theoretical and Experimental Characterization of Coplanar Waveguide Discontinuities for Filter Applications," *IEEE Trans. MTT* , vol. 39 , No. 5, May 1991, pp. 873-882.

[10] Dib, N. I., Katehi, P. B. "Modeling of Shielded CPW Discontinuities Using the Space Domain Integral Equation (SDIE)," *Journal of Electromagnetic Waves and Applications*, vol. 5 , No. 4/5, 1991, pp. 503-523.

[11] Dunleavy, L. P. "Discontinuity characterization in shielded microstrip: A theoretical and experimental study," Ph.D. Thesis, Radiation Laboratory, University of Michigan, Ann Arbor, 1988.

[12] Marcuvitz, N. *Waveguide Handbook*, vol. 10 of MIT Rad. Lab. Series, New York: McGraw-Hill, 1948.

[13] Kerr, A. R. "An Adjustable Short-Circuit for Millimeter Waveguides," *Electronics Division Internal Report No. 280*, National Radio Astronomy Observatory, Charlottesville, Virginia, July, 1988.